BLAST WAVE EXPERIMENTS AT Z*

T. E. Tierney IV, H. E. Tierney, R. G. Watt, G. C. Idzorek, R. R. Peterson, D. L. Peterson
Los Alamos National Laboratory, PO Box 1663, Mail Stop D410
Los Alamos, NM 87545
M. R. Lopez, and M. Jones
Sandia National Laboratories, PO Box 5800, Mail Stop 1193
Albuquerque, NM 87185-1193

Abstract

Blast waves (BWs) form when the wave speed of an initially diffusive, supersonic radiation wave becomes subsonic and creates a radiographically-visible, hydrodynamic shock wave. BWs are a novel diagnostic in radiation-flow, code validation experiments that use Sandia's Z-accelerator's dynamic hohlraum (DH) as a radiative source. The physics models being tested are sensitive to delivered energy and power changes of better than ±10%; therefore, precise in-situ radiative power and energy measurements are required for quantitative comparisons between simulation and experiment. The energy sensitive BW diagnostic complements bolometric and x-ray radiometric diagnostics in providing these measurements. Recent comparisons between BW qualification experiments and simulations have revealed a spatial dependence on the radiation source. We discuss the experimental design and sensitivities for the BW diagnostic and experimental results in comparison to simulations and other diagnostics.

I. INTRODUCTION

Blast waves are commonly observed in nature as associated with supernovae explosions, coronal mass ejections, and comet or meteor impacts on planets. As an example for supernovae, it is hypothesized that this phenomenon occurs as the shock break outs into the low density gas region surrounding the imploded star [1-2]. There the radiation emitted by the hydrodynamic shock becomes supersonic and out-runs the shock front due to the lower sound speed and opacity in that region [2]. As the radiation wave expands, its energy density lowers to a level where it travels transonically and a hydrodynamic wave can be seen as a density perturbation. This radiation driven blast wave can often be seen as the emission increases with density. Recent developments in pulsed radiation sources, such as those found at high fluence laser facilities and high power z-pinches, have enabled controlled measurements of blast wave properties.

Models for radiation transport through diffusive media are dependent upon the speed of radiation relative to the hydrodynamic sound speed of the heated material [3]. The simplest case is when the radiation wave is supersonic. The radiation wave propagates and heats new material too quickly to result in significant material motion. The pressure discontinuity at the interface between the heated and unheated material moves before the material can compensate by expanding into the unheated region.

Using a simple one-dimensional power law scaling, the radiation wave speed u_{rad} can be estimated as $u_{rad} \propto \varepsilon^{-6/20} t^{-19/20}$, where ε is the linear energy density of the wave and t is the time [3]. The material's hydrodynamic sound speed can also be estimated by $u_s \propto t^{-3/5}$. In the case of unconstrained radiation flow, the diffusive radiation wave slows with decreasing energy density due to its spherical expansion and losses to absorption into the medium. When the sound speed becomes comparable to the radiation wave speed, i.e., $u_{rad} \approx u_s$, a radiation-driven blast wave or Marshak wave forms, see Figure 1 [4]. The material near the front of the radiation wave begins to move into the colder medium in front. The hot material builds up a density perturbation at the pressure discontinuity.

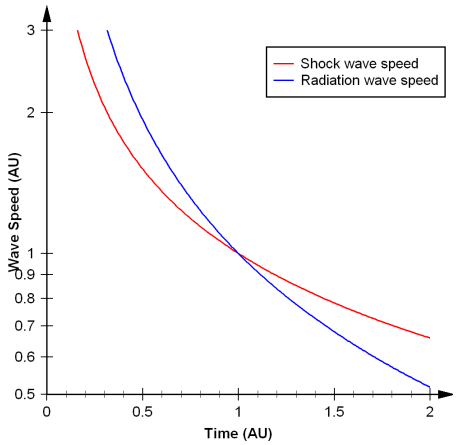

Figure 1 A notional plot highlighting how a radiation wave forms a blast wave in a material.

* This work was performed for the US Dept of Energy under the auspices of Los Alamos National Security, LLC. operator of Los Alamos National Laboratory under contract number DE-AC52-06NA25396

Report Documentation Page

Form Approved
OMB No. 0704-0188

1. REPORT DATE	2. REPORT TYPE	3. DATES COVERED
JUN 2007	**N/A**	**-**

4. TITLE AND SUBTITLE	5a. CONTRACT NUMBER
Blast Wave Experiments At Z	5b. GRANT NUMBER
	5c. PROGRAM ELEMENT NUMBER
6. AUTHOR(S)	5d. PROJECT NUMBER
	5e. TASK NUMBER
	5f. WORK UNIT NUMBER
7. PERFORMING ORGANIZATION NAME(S) AND ADDRESS(ES)	8. PERFORMING ORGANIZATION REPORT NUMBER
Sandia National Laboratories, Albuquerque, N.M. 87185, USA	
9. SPONSORING/MONITORING AGENCY NAME(S) AND ADDRESS(ES)	10. SPONSOR/MONITOR'S ACRONYM(S)
	11. SPONSOR/MONITOR'S REPORT NUMBER(S)

12. DISTRIBUTION/AVAILABILITY STATEMENT

Approved for public release, distribution unlimited

13. SUPPLEMENTARY NOTES

See also ADM002371. 2013 IEEE Pulsed Power Conference, Digest of Technical Papers 1976-2013, and Abstracts of the 2013 IEEE International Conference on Plasma Science. IEEE International Pulsed Power Conference (19th). Held in San Francisco, CA on 16-21 June 2013., The original document contains color images.

14. ABSTRACT

Blast waves (BWs) form when the wave speed of an initially diffusive, supersonic radiation wave becomes subsonic and creates a radiographically-visible, hydrodynamic shock wave. BWs are a novel diagnostic in radiation-flow, code validation experiments that use Sandias Z-accelerators dynamic hohlraum (DH) as a radiative source. The physics models being tested are sensitive to delivered energy and power changes of better than ±10%; therefore, precise in-situ radiative power and energy measurements are required for quantitative comparisons between simulation and experiment. The energy sensitive BW diagnostic complements bolometric and x-ray radiometric diagnostics in providing these measurements. Recent comparisons between BW qualification experiments and simulations have revealed a spatial dependence on the radiation source. We discuss the experimental design and sensitivities for the BW diagnostic and experimental results in comparison to simulations and other diagnostics.

15. SUBJECT TERMS

16. SECURITY CLASSIFICATION OF:			17. LIMITATION OF ABSTRACT	18. NUMBER OF PAGES	19a. NAME OF RESPONSIBLE PERSON
a. REPORT	b. ABSTRACT	c. THIS PAGE			
unclassified	**unclassified**	**unclassified**	**SAR**	**4**	

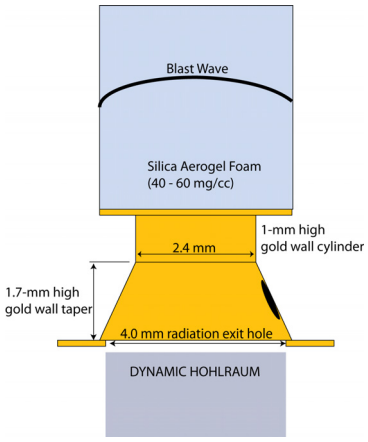

Figure 2 A silica aerogel foam rests above one axial end of the dynamic hohlraum.

This model simply illustrates the principal of the radiation-driven blast wave phenomenon, and the reader is encouraged to read more extensive derivations [2-5]. The analytic models are not easily solved through the transonic regime where the radiation transitions from supersonic to subsonic radiation transport.

II. EXPERIMENT SETUP

These experiments are performed at the 11.5 MJ Sandia National Laboratories- New Mexico Z-machine pulsed power facility [6]. The experiments use the Z *dynamic hohlraum* (DH) as an energetic x-ray source [7]. This source starts by passing current through two concentric (nested) arrays of tungsten wires. The outer array at 20-mm radius uses two-hundred forty 7.5-μm diameter wires, while the inner array at 10-mm radius uses one hundred twenty 7.5-μm diameter wires. These tungsten wires are weighted from above to retain tension on the arrays. The system has a return current conductor at 25-mm radius. These wires vaporize and implode cylindrically upon a 9.5-mm high, 5-mm diameter, 14 mg/cm^3 poly 4-methyl-1-pentane (TPX or ~ CH_2) plastic foam. When the tungsten hits the foam, a cylindrically-convergent radiating shock is generated that emits 70-120 kJ of quasi-blackbody x rays in each axial direction in a ~10-ns pulse with peak powers of 11-15 TW.

The blast wave targets rest above a 4-mm diameter radiation exit hole on the axial end of the TPX foam, see Figures 2 and 3. As radiation flows upward, it passes though a 1.7-mm high, tapered, 25-μm thick gold wall cone that is filled 20 ± 3 mg/cm^3 silica aerogel (SiO_2). Above this cone is a 20 ± 3 mg/cm^3 silica aerogel filled, 1-mm high, 2.4-mm inner diameter, 25-μm thick gold wall cylinder. On the cylinder rests a 4-mm diameter gold platform that supports a higher density (40-60 mg/cm^3) silica aerogel. This aerogel is the region where the blast wave forms after radiation emerges from the 2.4-mm diameter cylinder. A spatial fiducial grid is located on the target to provide a spatial calibration for radiography.

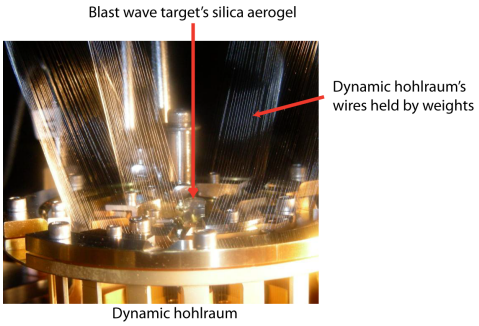

Figure 3 Photograph of the blast wave target above the dynamic hohlraum.

A 5-channel x-ray diode (XRD) array views the downward propagating axial emission from the dynamic hohlraum source [8]. This indirect measurement of input radiation has significant variability due to, possibly, the influx of tungsten plasma across the viewing aperture [7], current contacts between the wires and the transmission line [7], or a strong radial electric field [8]. The measured temperatures and time-integrated energy depositions are inconsistent with observations of target dynamics above the dynamic hohlraum. In follow-on experiments, a 1-mm diameter hole in the taper region of the target permits a view of the radiation source by a 5 to 8 channel XRD array above at 30° from vertical [9-10]. In general, the bottom XRD array peak radiation temperature T_{rad} measurements using a blackbody fit ranged from 150 to 180 eV with total energy delivery of 50-90 kJ. The blackbody fits converge in three to six iterations with a constraint of 5% residual on the fit. When measured from above through the taper hole in later experiments using the 30° XRD arrays, peak T_{rad} ranged from 180 to 220 eV.

The primary diagnostic for these experiments is the x-ray crystal imaging system pioneered by D. Sinars, et al., see Figure 4 [11]. This imaging diagnostic uses the Z-Beamlet laser [12] with approximately 1 kJ of laser energy in a 1-ns pulse, preceded by a ~0.3 kJ prepulse. By focusing to a ~0.15-mm diameter spot on a manganese foil, helium-like soft x-ray emission is produced. X rays with energies near 6.151 keV (λ = 2.016 Å) are focused

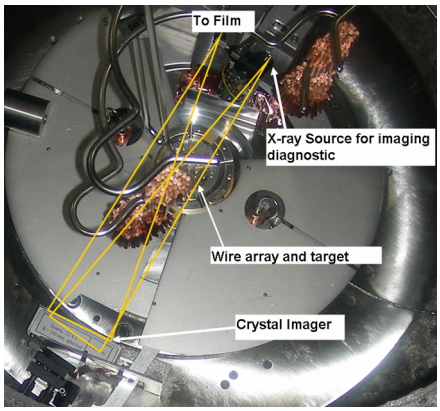

Figure 4 Photograph of the blast wave target with the x-ray imaging system.

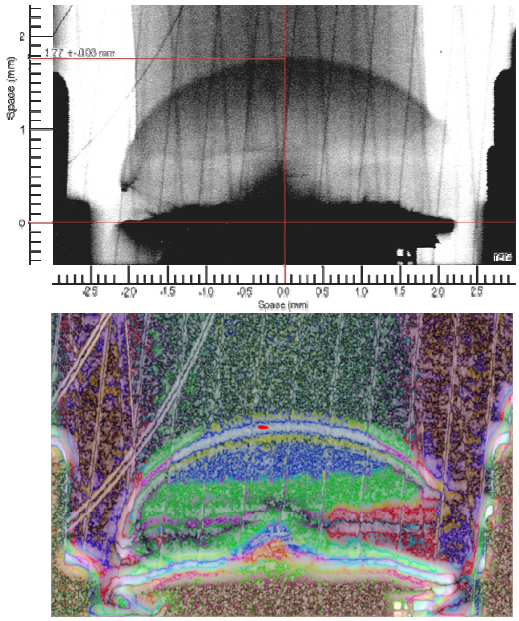

Figure 5 The radiographs are processed to extract the edges of the blast waves.

and Bragg-reflected by a spherically-bent (R = 250-mm) 2243 quartz crystal. The crystal provides a magnification near six times for spatial resolutions between 10 and 20 microns on a film pack. The x rays that are transported to the film are filtered by a layer of aluminized Kapton® poly(4,4'-oxydiphenylene-pyromellitimide) [$C_{16}H_{14}O_3$] and 50-μm beryllium [13]. A layer of double-emulsion Biomax-MS® film is used as a long-term recording media behind the beryllium foil [14]. Additionally, a Fuji TR image plate is placed between two 50-μm thick beryllium foils behind the Biomax film. The film and image plate combination provides good measures of spatial resolution, noise, and absolute flux. This Biomax films were scanned using a 10.5-micron by 10.5-micron aperture, while the image plate is scanned with a 25-micron aperture.

The x-ray image timing is given by measuring the time of leakage laser light that is transmitted through turning mirror prior to the final optics assembly, and referencing that with respect to the timing of peak DH emission. The radial emission is measured by a Kimfoil filtered channel on a radially-located 5-channel XRD array at the line-of-sight (LOS) 5-6 position. The axial emission timing is also referenced with respect to the LOS 5-6 XRD Kimfoil channel. Most images are taken 5-10 nanoseconds after peak axial power.

III. IMAGE ANALYSIS

The images obtained through the radiography system are post-processed using ENVI+IDL [15]. Preshot images of the undriven target provide spatial calibrations, "flat fields," and target anomaly information. Source intensity variations and imaging imperfections introduced by the x-ray crystal system are characterized with the preshot images. The weighted tungsten wires from the DH are in the field of view. These create poorly focused lines on the radiograph. The dynamic images are then median filtered. The Z-machine's x-ray background, obtained on a dynamic shot without the Z-beamlet laser driven source, is scaled to match intensities outside the typical laser-backlighter exposure region and subtracted from the dynamic image. In ENVI, occurrence measures are taken to produce a set of statistical images, including data range, mean, variance, entropy, and skewness. These statistical images are then recombined into a multi-channel synthesized multicolor image. A spectral angle mapper is then used to obtain texture correlations between image features and to generate a new enhanced image, see Figure 5. This technique works extremely well for low to moderate noise images, but care must be taken to retain the spatial resolution of the images. The enhanced edges are then extracted for comparison to simulations.

IV. SIMULATIONS

Simulations of the blast wave experiments are performed in two-dimensional R-Z geometry using the radiation-hydrodynamic code LASNEX [16]. The complicated dynamics of the DH are not modeled with the simulations. Due to the DH source's complexity and limited computing capacity, the problem is run with a simple line source placed just below the taper region of the target. The source is based upon time and space resolved measurements of the DH output performed from near on-axis using an x-ray imaging diagnostic [17]. Both the time and space dependence are included as a source to the model [18]. Detailed measurements of the angular dependence of the DH source emission have not been made and, therefore, are neglected. The metrologized target geometry, material compositions, and material densities are closely replicated in the R-Z geometry of the simulation's initial conditions. Simulated radiographs with photons at energy 6.151 keV are generated by postprocessing the simulations. In addition, plots of density are generated to monitor the position of the density perturbation, i.e. the blast wave position. For consistency, the simulated images are postprocessed using a similar methods as those used to extract the data from experimental images.

V. DISCUSSION

We performed six experiments from 2004 through 2006 with 40 mg/cm^3 and 60 mg/cm^3 silica aerogel foams. Experiments using 40 mg/cm^3 silica aerogel produced poor contrast on film for the blast wave positions. Except in one case where the wave formed partially outside the field of view, these images could be analyzed to extract the blast wave position. Target that used 60 mg/cm^3 silica aerogel exhibited improved contrast and prevented the appearance of blast waves outside the field of view. The contrast improvement is due to increased line-integrated density ρR and, thus, total x-ray absorption in the shock front. Also, the density increase results in a shorter

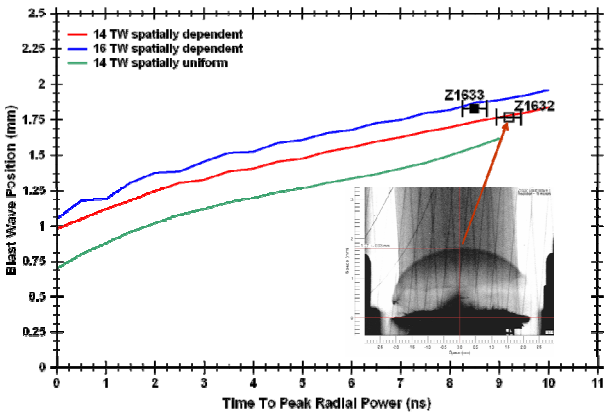

Figure 6 Simulated blast wave positions compared to experimental measurements.

Rosseland mean-free-path, which shortens the distance of propagation for the radiation wave. In all images, a jet begins to appear on-axis far behind the blast wave. The formation of this jet is currently being studied.

Spatially-dependent source simulations agree with the expected peak source powers of 14-16 TW, see Figure 6, measured using the XRD array located at 30° from vertical. These measurements viewed through a hole in the target's taper region on shots that immediately followed the blast wave experiments. In contrast, when a spatially-uniform source was used, the peak power required to produce the blast wave at the observed positions was between 19 and 21 TW. Such a power level would be impressive, but is certainly not realistic. It is interesting to note that the energy that is delivered to the foam is the same for both the spatially-uniform and spatially-dependent cases.

VI. SUMMARY

We developed a blast wave diagnostic using several series of experiments at the Sandia Z-facility. Sensitivities of the diagnostic to foam densities and computational techniques have been examined in detail. The blast wave diagnostic produces measurements in agreement with the energy sensitivity predictions reported by R. Peterson, et al. in Ref. [3].

VII. ACKNOWLEDGEMENTS

The authors acknowledge the support of the Z-Machine staff and crew in executing these experiments, especially Tom Sanford, Ray Mock, Ray Leeper, Gordon Leifeste, John Porter, Carlos Ruiz, Tommy Mulville, Richard Adams, and Guy Bennett. The feature extraction technique involved the support and guidance of ITT Visual Information Systems, in particular David Gorodetzky and Stephanie Staley.

VIII. REFERENCES

[1] L. Ensman and A. Burrows, "Shock breakout in SN 1987A," Astroph. J. **393**, p742 (1992); S.A. Zhekov, et al. "*CHANDRA* observations of shock kinematics in supernova remnant 1987A," Astrop. J. **628**, L127 (2005).

[2] Ya.B. Zel'dovich and Yu. P. Razier, *Physics of Shock Waves and High Temperature Hydrodynamic Phenomena*, (Academic Press, New York, 1966).

[3] R.R. Peterson, et al., "Blast wave radiation source measurement experiments on the Z Z-pinch facility," Phys. Plasmas **13**, 056901 (2006).

[4] R.E. Marshak, "Effect of radiation on shock wave behavior," Phys. Fluids **1**, 24 (1958).

[5] D. Mihalis and B. Weibel-Mihalis, *Foundations of Radiation Hydrodynamics*, (Dover Publications, New York, 1999); and, J.H. Hammer and M.D. Rosen, "A consistent approach to solving the radiation diffusion equation," Phys. Plasmas **10**, 1829 (2003).

[6] R.B. Spielman, et al., "Pulsed Power Performance of PBFA-Z," in *Proc. of the 11th IEEE International Pulsed Power Conference*, p.709, (1997).

[7] T.W.L. Sanford, et al., "Dynamics and Characteristics of a 215-eV Dynamic-Hohlraum X-Ray Source on Z," Phys. Plasmas **9**, 3573 (2002).

[8] G.C. Idzorek, T.E. Tierney, and R.G. Watt, "Radiation measurement accuracy of Z-dynamic hohlraums," in *Proc. of the 2007 IEEE Pulsed Power and Plasma Science Conference*, to appear, (2007).

[9] R.G. Watt, et al., "Blast wave measurements of ICF hohlraum energy loss at Z," in *Proc. of the 2007 IEEE Pulsed Power and Plasma Science Conference*, to appear, (2007).

[10] T.W.L. Sanford, *private communication* (2006).

[11] D. Sinars, et al., Rev. Sci. Instrum. **74**, 2202 (2003); and, D. Sinars, et al., Rev. Sci. Instrum. **75**, 3672 (2004).

[12] B.M. Van Wonterghem, et al., "System description and initial performance results for Beamlet," *Inertial Confinement Fusion Quarterly* (UCRL-LR-105821-95-1), **5** (1), 1 (1974); G.R. Bennett, et al., "X-ray imaging techniques on Z using the Z-Beamlet laser," Rev. Sci. Instrum. **72**, 657 (2001).

[13] "Dupont Kapton polyimide film general specifications," Dupont Bulletin GS-96-7 (1996), http://www2.dupont.com/Kapton/en_US/assets/downloads/pdf/Gen_Specs.pdf.

[14] G.R. Bennett, *private communication*, (2006); and, "Response model for Kodak Biomax-MS film to x rays," *LLE Review* **107**, (2006).

[15] ITT Visual Information Systems, Boulder, Colorado.

[16] G.B. Zimmermann and W.L. Kruer, "Numerical simulation of laser-initiated fusion," Comments Plasma Phys. Controlled Fusion **2**, 51 (1975).

[17] T.W.L. Sanford, et al., "Progress in z-pinch driven dynamic-hohlraums for high-temperature radiation-flow and ICF experiments at Sandia National Laboratory," Plasma Phys. Controlled Fusion **46**, B423 (2004).

[18] H.E. Tierney, et al., "Importance of radial distribution of drive energy for blast wave simulations," in preparation for submission to Phys. Plasmas (2007).